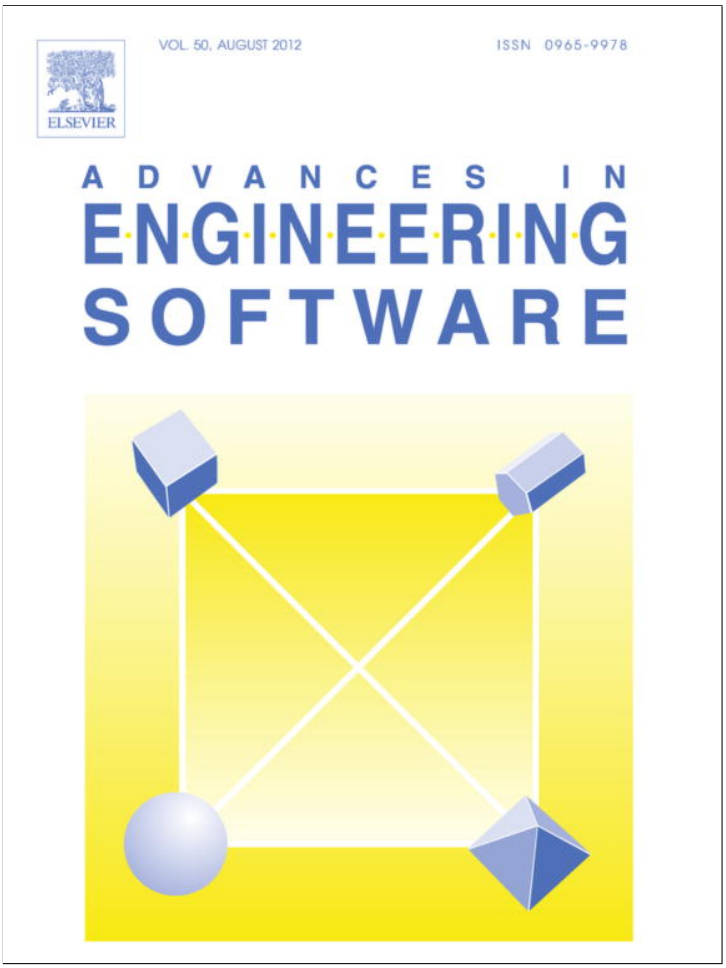

Advances in Engineering Software 50 (2012) 44–56

Contents lists available at SciVerse ScienceDirect

Advances in Engineering Software

journal homepage: www.elsevier.com/locate/advengsoft

Critical velocity of a uniformly moving load

Z. Dimitrovová *, A.F.S. Rodrigues

UNIC, Department of Civil Engineering, Universidade Nova de Lisboa, Portugal

ARTICLE INFO

Article history:
Available online 19 March 2012

Keywords:
Non-homogeneous foundation
Transverse vibration
Maximum displacement
Euler–Bernoulli beam theory
Timoshenko–Rayleigh beam theory
Modal expansion

ABSTRACT

An analysis of the critical velocity of a load moving uniformly along a beam on a visco-elastic foundation composed of one or two sub-domains is presented. The case study addressed is related to high-speed railway lines. A new formulation of the governing equations in the first order state-space form is proposed for the Timoshenko–Rayleigh beam. Differences in results obtained by Euler–Bernoulli and Timoshenko–Rayleigh beam theories are analysed. It is concluded that, in the case study considered, these differences are negligible. Critical velocities are obtained for load travelling on finite and infinite beams, with and without damping. A new relationship between the viscous damping coefficient and the modal damping ratio is derived and justified. Predictions about critical velocities established in [1] are confirmed numerically for cases not considered in [1], i.e. in cases when the load passes on infinite beams and when damping is considered.

1. Introduction

The response of rails to moving loads is of interest in the area of high-speed transportation. If simple geometries of the track and subsoil are considered, a theoretical concept that is based on the assumption that the track structure acts as a continuously supported beam (the rail) resting on a uniform layer of springs can be introduced. This layer of springs represents the underlying remainder of the track structure, composed of sleepers, ballast, subballast and subgrade. The stiffness of such spring layer along the length of the track is named as the track modulus, also referred to as the modulus of elasticity of the rail support. A single term representing the viscous damping of the foundation is usually added to the governing equations describing transverse vibrations of the rail induced by the moving load.

For such simplified models, analytical or semi-analytical solutions may be derived and thus several concerns related to railway lines can be quickly solved. Other advantages of simplified models are listed as follows: (i) only the main results are available, so they are simple to analyse; (ii) the results usually preserve parameter dependence, allowing for direct sensitivity analysis; (iii) numerical evaluation can be carried out only in places of interest, without following the full time history; (iv) high results precision is ensured within the simplified frame; (v) fast results evaluation is possible. However, due to the simplifying assumptions, it must be stressed that the results obtained reflect only an approximation of the real structural response to the moving load.

Since a considerable amount of studies have been published on this subject, only a few pioneering works are mentioned. Dynamic stresses in the beam structure were first solved by Krylov [2] and later by Timoshenko [3]. Transverse vibrations in a simply supported beam traversed by a constant force moving at a constant velocity were presented by Inglish [4], Lowan [5] and, later on, other solutions have been given by Koloušek [6] and Frýba [7]. In these approaches the deflection field is expressed as an infinite sum of normal modes. Each mode contribution can be obtained by methods of integral transformation, [8].

Solutions for infinite beams were first presented by Timoshenko [9]. The Fourier transform is used for solving the ordinary differential equation. In [10] the effect of the foundation's viscous damping on the response was also discussed. The case of a load variable over time is presented in [11]. The conventional elastic foundation can sustain both compression as well as tension when the beam deforms. The steady state deformation of an infinite beam on a tensionless elastic foundation under a moving load was first studied in [12]. An important comparison between finite and infinite beam characteristics is presented in [13].

When dealing with non-homogeneous supports or foundation stiffness, it is relevant to mention a review by Vesnitskii and Metrikine on transition radiation in mechanics [14]. According to this work, when the load passes at a constant velocity over a discontinuity in the supporting structure, additional vibrations, conventionally referred to as transition radiation, are generated. These vibrations can significantly amplify the beam's deflection field. In [15], transition radiations in elastic systems are analysed. Other analytical studies addressing the foundation stiffness change are presented in [16]. The ones based on the concept of the dynamic stiffness matrix are given in [1,17,18].

* Corresponding author. Address: Department of Civil Engineering, Faculade de Ciencias e Tecnologia, Universidade Nova, 2829-516 Caparica, Portugal.
E-mail address: zdim@fct.unl.pt (Z. Dimitrovová).

0965-9978/$ - see front matter © 2012 Civil-Comp Ltd and Elsevier Ltd. All rights reserved.
doi:10.1016/j.advengsoft.2012.02.011

In this paper, the analysis of critical velocity of a load moving uniformly along a beam on visco-elastic foundation is presented. The critical velocity, in the context of this paper, is defined as the load velocity inducing the beam's highest deflections directed downward and/or upward. This velocity is obtained by a parametric analysis during which extreme displacements are determined for each considered velocity. Analyses are carried out on finite as well as infinite beams, on beams for which the foundation is composed of one or two homogeneous sub-domains (see description in Section 2) and with or without damping influence. Free vibrations on finite beams after the load has already left the structure are also analysed. Results related to beams composed of a single sub-domain are obtained by adopting Euler–Bernoulli (E–B) and Timoshenko–Rayleigh (T–R) theories. Due to negligible differences in results, only E–B beams composed of two sub-domains are considered further. Conclusions taken on the beams composed of two sub-domains allow for generalization to several sub-domains.

Several authors presented results obtained on finite simply supported beams [19,20] or clamped beams [21] as the ones that correspond to infinite beams. In these works no care is taken to address the issue of reflected waves. The beam lengths introduced are 30 m, 62.4 m and 32.5 m, respectively, which cannot be considered very long. In this paper it is shown that results obtained on a finite beam on soft elastic foundation cannot be interchanged with results obtained on a corresponding infinite beam. Even a beam longer than specified above (200 m) is considered in this paper. Along with the analysis of critical velocity, the main goal of the study presented in this paper is to identify differences in results of finite and infinite beams in terms of: (i) the maximum displacement gradient with respect to the load velocity; (ii) the effect of transition radiation; (iii) the damping influence.

The consideration of realistic damping behaviour is not a simple task. Total damping should include the material damping and the geometrical (radiation) damping, that is, the geometrical dissipation due to wave propagation into the subsoil. It was proven in [22] that the models represented by a low number of parameters like the one used in this paper cannot correctly represent the geometrical dissipation. Material damping should encompass both internal friction in the beam as well as damping of the geomaterial representing the foundation. According to experiments, material damping of geomaterials is frequency independent [23], thus it should be modelled as hysteretic damping. Often viscous damping is considered instead, because it leads to a convenient form of the equation of motion [23], but then the energy loss per cycle is dependent upon the excitation (or response) frequency. Due to several simplifying assumptions already adopted, a more realistic damping model would not improve accuracy significantly, therefore only viscous damping is considered. The value of the critical viscous damping coefficient related to infinite beams is very often introduced in an approximate way [24]. The correct formulation for infinite Euler–Bernoulli (E–B) beams is given in [7], and a new (not yet published) formula is derived in this paper for the critical damping of infinite Timoshenko–Rayleigh (T–B) beam.

Along the developments presented in this paper, new formulations are given for: (i) the first order state-space form of T–R beam; and (ii) for the relation between the viscous damping constant and the modal damping ratio assuring the same level of damping in lightly damped finite beam structures.

The critical velocities determined for the case study considered are still unattainable by nowadays trains. Nevertheless, results presented in this paper have practical importance because they show values of extreme displacements as a function of velocity. Especially augmented displacements directed upward, that aggravate track deterioration, should be avoided in railway applications.

The paper is organized in the following way: in Section 2, a general description of the problem and the simplifying assumptions are stated. In Section 3, the case study is defined. In Section 4, finite and infinite beams composed of one sub-domain are analysed under the assumption of E–B and T–R beam theory. In Section 5, finite and infinite beams composed of two sub-domain are analysed under the assumption of E–B beam theory. In Section 6, numerical results are presented. Conclusions are drawn in Section 7.

2. General description of the problem

A uniform motion of a constant single vertical force along a horizontal beam on a linear visco-elastic foundation is assumed. The foundation is modelled as distributed springs and dashpots. The beam is homogeneous with a uniform cross section made of a linear elastic material and its damping is proportional to the velocity of vibration. The load's inertia is neglected.

Finite simply supported and infinite beams will be addressed. The foundation will be composed of one or two sub-domains with uniform properties. In Fig. 1, a finite simply supported beam on a foundation composed of two sub-domains is shown. P stands for the moving force, v is its constant velocity, x and w are spatial coordinate and vertical deflection. The deflection is assumed positive when oriented downward and is measured from the equilibrium position, when the beam is only loaded with its own weight. At zero time ($t = 0$) the load is located at the origin of the spatial coordinate x.

The critical velocity of the single load will be addressed, examined and compared for finite and infinite beams on a homogeneous foundation (foundation composed of a single sub-domain) and on a foundation composed of two sub-domains. Conclusions drawn are possible to extend to situations with more foundation sub-domains. For the sake of simplicity, the term "sub-domain" will be used not only for the foundation, but also for the corresponding beam structure. Transverse vibrations induced by the load are solved by the normal-mode analysis. The natural frequencies are obtained numerically exploiting the concept of the global dynamic stiffness matrix. This ensures that the frequencies obtained are accurate. For infinite beams composed of two sub-domains the method described in [17] is adopted. Results on homogeneous infinite beams are obtained according to [7,24].

In this context, it is necessary to review previous works. In [1], the load critical velocity on undamped finite beams composed of

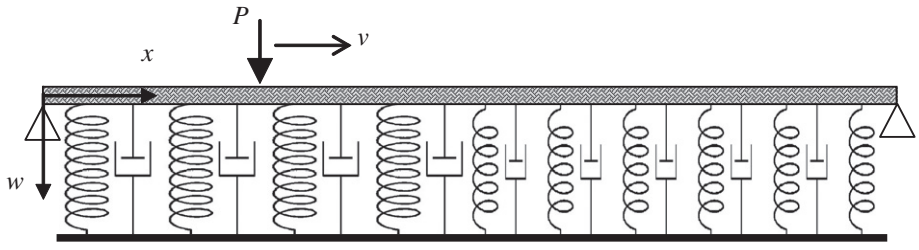

Fig. 1. Simply supported beam on a foundation composed of two sub-domains.

two sub-domains is examined, but the velocity step in the parametric analysis is quite large and therefore the effect of waves reflection is not accurately demonstrated. Moreover, extreme displacements are not separated according to the load position. Such a separation is very important, because it shows that sometimes higher displacements in the first sub-domain are attained when the force is already passing over the second sub-domain, as a result of transition radiation and waves reflection. A method that allows dealing with infinite beams by modal expansion method is presented in [17]. In [18], the effect of damping on finite beams composed of two sub-domains is studied. It was concluded in [1] that, in beams composed of two sub-domains, the velocities that correspond to critical velocities of the sub-domains considered separately, are themselves critical in both sub-domains. This conclusion will be analysed in other cases not considered in [1].

It was justified in [1,17] that the modal expansion of a transient displacement of a beam on an elastic foundation requires a significant number of vibration modes until an acceptable accuracy is achieved. In this paper, 300 modes will be used for finite beams and 800–1300 modes in the method from [17] when dealing with infinite beams composed of two sub-domains. There are no numerical difficulties in results evaluation related to simply supported beam composed of single sub-domain. However, when different boundary conditions and/or beams composed of more sub-domains are considered, one must be aware of numerical errors in higher mode shapes evaluation. These problems are first mentioned in [25], where an alternative formulation of mode shapes is suggested. In [26], the error in mode shape evaluation is estimated considering double precision calculation. We suggested in [17] an alternative formulation that also performs well in double precision even for a significant number of modes and, moreover, keeps the evaluation mostly within the real domain. Nevertheless, very high modes require evaluation in software with adaptable number of digits precision without any link to the computer specified value. In addition, such software must handle very high and low numbers, which is necessary for high natural frequencies determination. Natural frequencies search and numerical evaluation of analytical formulae was programmed as interconnected modules of MAPLE [27] and MATLAB [28] software. The objective was to combine the high precision of Maple with the fast evaluation of Matlab software.

3. Case study

The case study addressed in this paper is related to high-speed railways. As stated in the Introduction, a beam on a visco-elastic foundation is considered. Finite and infinite beams will be analysed. The length of the finite beam is taken as 200 m. For the sake of simplicity and easy comparison of analytical values, the finite beam is simply supported.

UIC60 rail is used to model the beam (introduced numerical data according to [29] are summarized in Table 1). The load applied has a total axle mass of 17,000 kg corresponding to a locomotive of the Thalys high-speed train, thus the force used is $P = 83.4$ kN. Two case studies were considered. The first case study, discussed in Sections 4 and 6.1, is a beam composed of a single sub-domain with a relatively soft foundation of $k = 0.25$ MN/m^2. The second case study is a beam composed of two sub-domains, the first one with a soft foundation ($k_1 = 0.25$ MN/m^2) and the second one with a stronger foundation ($k_2 = 0.5$ MN/m^2), and it is analysed in Section 5 and 6.2. These values are taken according to [16], in which the beam is modelled as two UIC60 rails, as also in [1,17]. Nevertheless, it is more common to use just one rail [13,24] because of the definition of the track modulus that corresponds to the Winkler foundation stiffness of a single rail. The effect of axial force will not be taken into account. In Fig. 2, the case study corresponding to the finite undamped beam composed of two sub-domains is shown.

Table 1
Characteristics of UIC60 rail according to [29].

Property	Beam (UIC60 rail)
Young's modulus E (GPa)	210
Poisson's ratio ν	0.3
Shear modulus $G = \frac{E}{2(1+\nu)}$ (GPa)	80.769
Density ρ (kg/m^3)	7800
Transverse cross-sectional area A (m^2)	76.84×10^{-4}
Shear coefficient κ	0.41
Area moment of inertia I (m^4)	3055×10^{-8}
Radio of gyration r (m)	0.063
Bending stiffness EI (MN m^2)	6.4155
Shear stiffness $G\bar{A} = \kappa GA$ (MN)	254.46
Mass per unit length μ (kg/m)	59.9352

4. Beam composed of a single sub-domain

4.1. Infinite beam

The infinite homogeneous beam on visco-elastic foundation subjected to a moving load has been studied over the years by several authors, such as [7,13,24]. The analytical solution indicates a symmetric deflection shape in the undamped case, with the maximum displacement value at the actual load position for subcritical velocities. At critical velocity, the analytical displacement tends to infinity. Zero deflection in the actual load position is verified for supercritical velocities [7].

Critical velocity v_{cr} is given for E–B and T–R beams by:

$$v_{cr}^{E-B} = \sqrt[4]{\frac{4kEI}{\mu^2}} \tag{1}$$

$$v_{cr}^{T-R} = \sqrt{\frac{1}{\mu(kr^2 - G\bar{A})^2}\left(k(EI(kr^2 - G\bar{A}) - 2r^2G\bar{A}^2) + 2G\bar{A}\sqrt{kG\bar{A}}\sqrt{kr^4G\bar{A} - EI(kr^2 - G\bar{A})}\right)} \tag{2}$$

The numerical values for the case study are $v_{cr}^{E-B} = 205.573$ m/s and $v_{cr}^{T-R} = 205.237$ m/s. As the proximity of these values indicates, there are no visible differences in the deflection shapes on E–B and T–R beams. For the case study specified, some deflection shapes are shown in Fig. 3, obtained with the E–B beam theory.

When damping is present, infinite displacement never occurs and the deflection shape is asymmetric. The viscous critical damping coefficient c_{cr} causes an onset of the case when the deflection shape behind the load does not have a harmonic component. The critical damping is often associated with the approximate value of $2\sqrt{k\mu}$ [24], due to the analogy with one-degree-of-freedom systems. The correct value must be determined from the condition

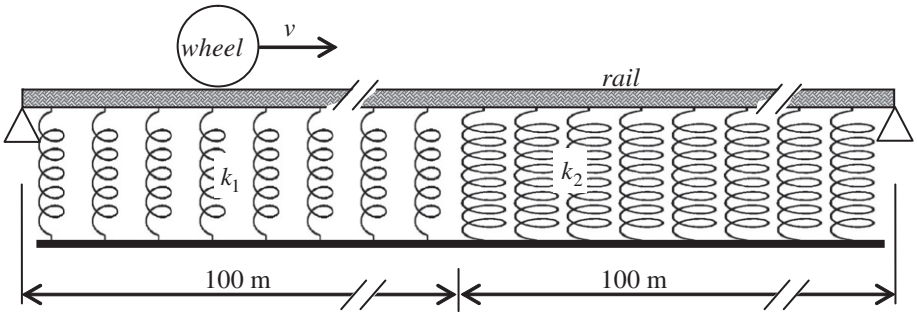

Fig. 2. Case study corresponding to finite undamped beam composed of two sub-domains.

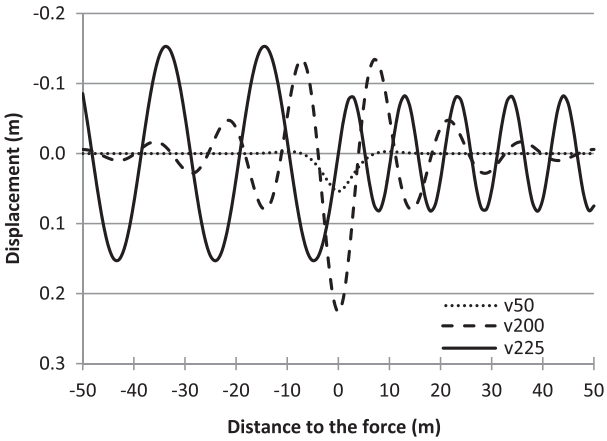

Fig. 3. Infinite beam, load passage at 50, 200, and 225 m/s, respectively.

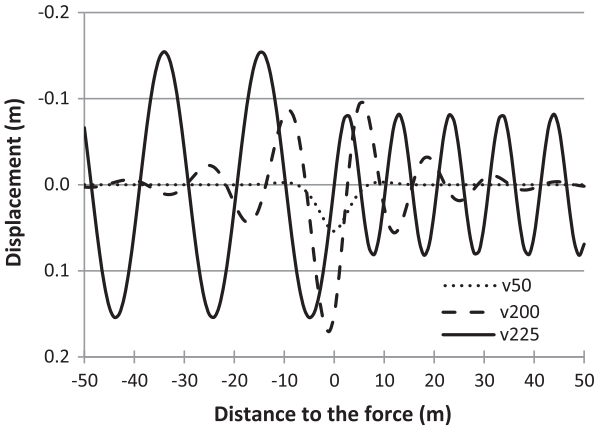

Fig. 4. Infinite beam, load passage at 50, 200, and 225 m/s, respectively, 5% of the critical damping.

that leads to no harmonic shape behind the load, therefore it must depend on velocity v. For E–B beam it is [7]:

$$c_{cr}^{E-B} = \frac{2\sqrt{k\mu}}{\alpha}\sqrt{\frac{2}{27}(-\alpha^2+\sqrt{\alpha^4+3})(2\alpha^2+\sqrt{\alpha^4+3})} \tag{3}$$

where

$$\alpha = v/v_{cr}^{E-B} \tag{4}$$

For T-R beam such a condition is more complicated, but the critical damping coefficient can also be expressed analytically:

$$c_{cr}^{T-R} = \frac{1}{2}\frac{k\bar{GA} - 3a^4 D_1 D_2 + a^2\left(kD_2 + \bar{GA}D_1 - \bar{GA}^2\right)}{a^3 vD_2} \tag{5}$$

where

$$a = \sqrt{\frac{I_1}{3}+\frac{2}{3}\sqrt{I_1^2-3I_2}\cos\left(\theta+\frac{4\pi}{3}\right)},$$

$$\theta = \frac{1}{3}\arccos\left(\frac{2I_1^3-9I_1I_2+27I_3}{2(I_1^2-3I_2)^{3/2}}\right)$$

$$D_1 = \bar{GA}-\mu v^2, \quad D_2 = EI-\mu v^2 r^2 \tag{6}$$

$$I_1 = \frac{2\bar{GA}D_1 - kD_2 + \bar{GA}^2}{D_1D_2}, \quad I_2 = -\bar{GA}\frac{\left(2kD_2 - \bar{GA}D_1 + \bar{GA}^2\right)}{D_1D_2^2},$$

$$I_3 = -\frac{k\bar{GA}^2}{D_1D_2^2}$$

Eq. (5) is a new, not yet published, result. Deflection shapes are shown in Fig. 4 for 5% of the critical damping value. Results on E–B beam are also shown. Results on T–R beam are overlaid, with no visible differences.

A parametric analysis with respect to the velocity was performed, and extreme displacement values were extracted. Small differences between values obtained on E–B and T–R beams were noticed. Their origin can be attributed to the small difference in critical velocity. For instance in the undamped case, shifting the results in a way to match the critical velocities, all differences laid within 2% until the critical velocity and then they increased to 4.5% for the velocity of 300 m/s. Corresponding graphs will be presented later on, as they will serve for the comparison with the finite beam results.

4.2. Finite simply supported beam

In this section, the governing equations for T–R beam are reviewed. A new formulation in the first order state-space form is proposed. This formulation is self-adjoint and therefore leads to a new definition of a modal mass in a generalized form.

Let a simply supported T–R beam on visco-elastic foundation composed of single sub-domain be assumed. The coupled governing equations for bending rotation $\psi(x,t)$ and transverse deflection $w(x,t)$ read as:

$$\frac{\partial}{\partial x}\left(EI\frac{\partial\psi(x,t)}{\partial x}\right)+\bar{GA}\left(\frac{\partial w(x,t)}{\partial x}-\psi(x,t)\right)-\mu r^2\frac{\partial^2\psi(x,t)}{\partial t^2}=0 \tag{7}$$

$$\mu\frac{\partial^2 w(x,t)}{\partial t^2}-\frac{\partial}{\partial x}\left(\bar{GA}\left(\frac{\partial w(x,t)}{\partial x}-\psi(x,t)\right)\right)-\frac{\partial}{\partial x}\left(N\frac{\partial w(x,t)}{\partial x}\right)+kw(x,t)+c\frac{\partial w(x,t)}{\partial t}=p(x,t) \tag{8}$$

where N is the axial force (positive as traction) and $p(x,t)$ is the general loading term, which for the case of a single force moving at constant velocity v is given by $P\delta(x-vt)$, where δ is the Dirac delta function. The damping coefficient c encompasses both the damping of the distributed dashpots as well as the material damping of the beam. Boundary conditions are

$$w(0,t)=0,\quad w(L,t)=0,\quad \left.\frac{\partial M(x,t)}{\partial x}\right|_{x=0}=0,\quad \left.\frac{\partial M(x,t)}{\partial x}\right|_{x=L}=0\quad \forall t \tag{9}$$

where L corresponds to the total beam length and the flexural moment M is given by

$$M(x,t)=-EI\frac{\partial\psi(x,t)}{\partial x} \tag{10}$$

Homogeneous initial conditions will be assumed for the sake of simplicity:

$$w(x,0)=0,\quad \left.\frac{\partial w(x,t)}{\partial t}\right|_{t=0}=0,\quad \psi(x,0)=0,\quad \left.\frac{\partial\psi(x,t)}{\partial t}\right|_{t=0}=0 \tag{11}$$

For uniform beam characteristics, Eqs. (7) and (8) can be simplified and uncoupled for w and ψ, yielding two analogous fourth order equations in space and time (variables x and t are omitted for the sake of simplicity):

$$EI\frac{\partial^4 w}{\partial x^4}-\mu r^2\frac{\partial^4 w}{\partial t^2\partial x^2}+\left(1-\frac{EI}{G\bar{A}}\frac{\partial^2}{\partial x^2}+\frac{\mu r^2}{G\bar{A}}\frac{\partial^2}{\partial t^2}\right)\times\left(\mu\frac{\partial^2 w}{\partial t^2}-N\frac{\partial^2 w}{\partial x^2}+kw+c\frac{\partial w}{\partial t}\right)=p+\frac{\mu r^2}{G\bar{A}}\frac{\partial^2 p}{\partial t^2}-\frac{EI}{G\bar{A}}\frac{\partial^2 p}{\partial x^2} \tag{12}$$

$$EI\frac{\partial^4\psi}{\partial x^4}-\mu r^2\frac{\partial^4\psi}{\partial x^2\partial t^2}+\left(1-\frac{EI}{G\bar{A}}\frac{\partial^2}{\partial x^2}+\frac{\mu r^2}{G\bar{A}}\frac{\partial^2}{\partial t^2}\right)\times\left(\mu\frac{\partial^2\psi}{\partial t^2}-N\frac{\partial^2\psi}{\partial x^2}+k\psi+c\frac{\partial\psi}{\partial t}\right)=\frac{\partial p}{\partial x} \tag{13}$$

A commonly used technique for transient response determination is the modal expansion of w and ψ in series of undamped modes. Undamped modes in this case form complete space and the form of viscous damping introduced will not prevent uncoupling in modal space. The displacement field is then given by:

$$w(x,t)=\sum_j q_j(t)w_j(x) \tag{14}$$

where $q_j(t)$ and $w_j(x)$ are the jth modal coordinate and the jth undamped vibration mode.

The solution $w(x,t)$ is unique. Therefore, if after adopting some assumptions the resulting form given by Eq. (14) will fulfil the governing equations, it is possible to conclude that these assumptions imposed no restriction on the solution itself, only on the form how it is expressed.

One can determine undamped vibration modes by assuming that the solution of homogenous Eq. (12) without the damping term is separable in time and space, and that it has a form of harmonic vibrations $w(x,t)=w(x)e^{i\omega t}$, where $i=\sqrt{-1}$ and ω is the circular frequency of these vibrations. Similar relations hold for internal forces. Then:

$$\left(1+\frac{N}{G\bar{A}}\right)\frac{d^4 w}{dx^4}+\left(\frac{1}{EI}\left(\mu r^2\omega^2\left(1+\frac{N}{G\bar{A}}\right)-N\right)+\frac{1}{G\bar{A}}(\mu\omega^2-k)\right)\frac{d^2 w}{dx^2}-\frac{1}{EI}\left(1-\frac{\mu r^2\omega^2}{G\bar{A}}\right)(\mu\omega^2-k)w=0 \tag{15}$$

The same equation can be obtained for ψ. Boundary conditions remain coupled:

$$w(0)=0,\quad w(L)=0,\quad \left.\frac{d\psi(x)}{dx}\right|_{x=0}=0,\quad \left.\frac{d\psi(x)}{dx}\right|_{x=L}=0 \tag{16}$$

The wave number equation can be written in the following form [13,24]:

$$s^4+As^2+B=0 \tag{17}$$

where

$$A=\left(\frac{1}{EI}\left(\mu r^2\omega^2\left(1+\frac{N}{G\bar{A}}\right)-N\right)+\frac{\mu\omega^2-k}{G\bar{A}}\right)/\left(1+\frac{N}{G\bar{A}}\right) \tag{18}$$

$$B=-\frac{1}{EI}\left(1-\frac{\mu r^2\omega^2}{G\bar{A}}\right)(\mu\omega^2-k)/\left(1+\frac{N}{G\bar{A}}\right) \tag{19}$$

Four complex wave numbers correspond to each natural frequency. Their form is:

$$s_1=\sqrt{-\frac{A}{2}-\sqrt{\left(\frac{A}{2}\right)^2-B}},\quad s_2=\sqrt{-\frac{A}{2}+\sqrt{\left(\frac{A}{2}\right)^2-B}}$$
$$s_3=-\sqrt{-\frac{A}{2}-\sqrt{\left(\frac{A}{2}\right)^2-B}},\quad s_4=-\sqrt{-\frac{A}{2}+\sqrt{\left(\frac{A}{2}\right)^2-B}} \tag{20}$$

thus the mode shape, bending rotation and flexural moment are written as:

$$w(x)=\sum_{l=1}^{4}C_l e^{s_l x},\quad \psi(x)=\sum_{l=1}^{4}C_l\hat{s}_l e^{s_l x},\quad M(x)=-EI\sum_{l=1}^{4}C_l\hat{s}_l s_l e^{s_l x} \tag{21}$$

where

$$\hat{s}_l=s_l+\frac{1}{G\bar{A}s_l}\left(Ns_l^2+\mu\omega^2-k\right)=\frac{G\bar{A}s_l}{G\bar{A}-EIs_l^2-\mu r^2\omega^2},\ l=1,\ldots,4 \tag{22}$$

and the vertical reaction force is given by:

$$V(x)=G\bar{A}\left(\frac{dw}{dx}-\psi\right)+N\frac{dw}{dx}=G\bar{A}\left(\sum_{l=1}^{4}C_l(s_l-\hat{s}_l)e^{s_l x}\right)+N\left(\sum_{l=1}^{4}C_l s_l e^{s_l x}\right) \tag{23}$$

which can also be written as:

$$V(x)=EI(\hat{s}_1\hat{s}_3(C_1 s_3 e^{s_1 x}+C_3 s_1 e^{s_3 x})+\hat{s}_2\hat{s}_4(C_2 s_4 e^{s_2 x}+C_4 s_2 e^{s_4 x})) \tag{24}$$

Constants C_l, $l=1,\ldots,4$ must verify the boundary conditions. However, as the system of equations is homogeneous, its determinant (named as the characteristic equation) must be set to zero. The roots of this equation, ω_j, are the natural frequencies.

For $N=0$, Eqs. (18) and (19) can be simplified to:

$$A=\frac{\mu r^2\omega^2}{EI}+\frac{\mu\omega^2-k}{G\bar{A}} \tag{25}$$

$$B=-\frac{1}{EI}\left(1-\frac{\mu r^2\omega^2}{G\bar{A}}\right)(\mu\omega^2-k) \tag{26}$$

If

$$\frac{k}{\mu}<\omega^2<\frac{G\bar{A}}{\mu r^2} \tag{27}$$

then A is positive and B is negative and it is possible to keep the analysis within the real domain, for instance by defining:

$$\lambda_1 = L\sqrt{-\frac{A}{2}+\sqrt{\left(\frac{A}{2}\right)^2-B}}, \quad \lambda_2 = L\sqrt{\frac{A}{2}+\sqrt{\left(\frac{A}{2}\right)^2-B}},$$
$$\hat{\lambda}_1 = \lambda_1 + \frac{(\mu\omega^2-k)L^2}{G\bar{A}\lambda_1}, \quad \hat{\lambda}_2 = \lambda_2 - \frac{(\mu\omega^2-k)L^2}{G\bar{A}\lambda_2} \tag{28}$$

$$w(x) = C_1\cosh\left(\frac{\lambda_1}{L}x\right) + C_2\sinh\left(\frac{\lambda_1}{L}x\right) + C_3\cos\left(\frac{\lambda_2}{L}x\right) + C_4\sin\left(\frac{\lambda_2}{L}x\right)$$

$$\psi(x) = C_1\hat{\lambda}_1\cosh\left(\frac{\lambda_1}{L}x\right) + C_2\hat{\lambda}_1\sinh\left(\frac{\lambda_1}{L}x\right) + C_3\hat{\lambda}_2\cos\left(\frac{\lambda_2}{L}x\right) + C_4\hat{\lambda}_2\sin\left(\frac{\lambda_2}{L}x\right) \tag{29}$$

For a simply supported beam, $C_1 = C_2 = C_3 = 0$ and the characteristic equation is $\sin((\lambda_2 x)/L)=0$, thus $\lambda_{2j} = j\pi$, $j = 1,2,\ldots$, regardless of whether theory T–R or E–B is assumed. The mode shape for simply supported beam is therefore:

$$w_j(x) = \sin\left(\frac{j\pi}{L}x\right) \tag{30}$$

and the natural frequency is given by the following relations for E–B and T–R beams:

$$\omega_j^{E-B} = \sqrt{\left(\frac{j\pi}{L}\right)^4\frac{EI}{\mu}+\frac{k}{\mu}} \tag{31}$$

$$(\omega_j^{T-R})^2 = \frac{G\bar{A}}{2\mu r^2}\left\{1+\frac{kr^2}{G\bar{A}}+\left(\frac{j\pi}{L}\right)^2\left(\frac{EI}{G\bar{A}}+r^2\right) - \left(\left(1-\frac{kr^2}{G\bar{A}}\right)^2 - 2\frac{kr^2}{G\bar{A}}\left(\frac{j\pi}{L}\right)^2\left(\frac{EI}{G\bar{A}}-r^2\right) + 2\left(\frac{j\pi}{L}\right)^2\left(\frac{EI}{G\bar{A}}+r^2\right) + \left(\frac{j\pi}{L}\right)^4\left(\frac{EI}{G\bar{A}}-r^2\right)^2\right)^{1/2}\right\} \tag{32}$$

The second inequality in Eq. (27) means that, for the case study specified

$$\omega_j < \sqrt{\frac{G\bar{A}}{\mu r^2}} = 32,678 \text{ rad/s} \tag{33}$$

which is clearly satisfied for this particular application. Regarding the first inequality in Eq. (27), for E–B beams it is obvious. For T–R beam and the case study:

$$\sqrt{\frac{k}{\mu}} = 64.58461 < \omega_1^{T-R} = 64.58463 \text{ rad/s} \tag{34}$$

It can however happen that the first inequality in T–R beam is not fulfilled. Then, the mode shape given by Eq. (30) for $j = 1$ does not have the lowest natural frequency. More details can be found in [30].

Eqs. (12) and (13) are fourth order in time, therefore they are not convenient for determination of modal coordinates, because of the assumption of harmonic vibrations. It is more convenient to separate the equations and write them in the first order state-space form.

A not yet published formulation of Eqs. (7) and (8) in the first order state-space form is suggested (similarly as in [31]) as:

$$\begin{bmatrix} G\bar{A}-EI\frac{\partial^2}{\partial x^2} & -G\bar{A}\frac{\partial}{\partial x} & 0 & 0 \\ G\bar{A}\frac{\partial}{\partial x} & -N\frac{\partial^2}{\partial x^2}-G\bar{A}\frac{\partial^2}{\partial x^2}+k & 0 & 0 \\ 0 & 0 & -\mu r^2 & 0 \\ 0 & 0 & 0 & -\mu \end{bmatrix}\cdot\begin{Bmatrix}\psi(x,t)\\ w(x,t)\\ \vartheta(x,t)\\ \tau(x,t)\end{Bmatrix} + \begin{bmatrix} 0 & 0 & \mu r^2 & 0 \\ 0 & c & 0 & \mu \\ \mu r^2 & 0 & 0 & 0 \\ 0 & \mu & 0 & 0 \end{bmatrix}\cdot\frac{\partial}{\partial t}\begin{Bmatrix}\psi(x,t)\\ w(x,t)\\ \vartheta(x,t)\\ \tau(x,t)\end{Bmatrix} = \begin{Bmatrix}0\\ p(x,t)\\ 0\\ 0\end{Bmatrix} \tag{35}$$

where $\vartheta(x,t)$ and $\tau(x,t)$ are defined according to:

$$\vartheta(x,t) = \frac{\partial}{\partial t}\psi(x,t), \quad \tau(x,t) = \frac{\partial}{\partial t}w(x,t) \tag{36}$$

It is important to realize that the operator matrix is self-adjoint under the assumption of homogeneous boundary conditions. Then two orthogonality relations for damped vibration modes can be derived as:

$$\int_{x=0}^{L}\left(\psi_k(x)(G\bar{A}\psi_j(x) - EI\frac{d^2\psi_j(x)}{dx^2} - G\bar{A}\frac{dw_j(x)}{dx}) + w_k(x)\left(G\bar{A}\frac{d\psi_j(x)}{dx} - N\frac{d^2w_j(x)}{dx^2} - G\bar{A}\frac{d^2w_j(x)}{dx^2} + kw_j(x)\right) + \omega_k\omega_j\mu r^2\psi_k(x)\psi_j(x) + \omega_k\omega_j\mu w_k(x)w_j(x)\right)dx = \delta_{kj}D_j \tag{37}$$

$$\int_{x=0}^{L}(i\mu r^2(\omega_k+\omega_j)\psi_k(x)\psi_j(x) + i\mu(\omega_k+\omega_j)w_k(x)w_j(x) + cw_k(x)w_j(x))dx = \delta_{kj}H_j \tag{38}$$

where δ_{kj} is the Kronecker delta. Eqs. (37) and (38) are connected by

$$D_k + i\omega_k H_k = 0 \tag{39}$$

which allows introduction of the modal mass in a generalized form as:

$$D_k = -i\omega_k H_k = 2\omega_k^2 M_k^G$$
$$M_k^G = \int_{x=0}^{L}\left(\mu w_k^2(x) + \mu r^2\psi_k^2(x) + \frac{c}{2i\omega_k}w_k^2(x)\right)dx \tag{40}$$

By carrying out the modal analysis, the solution is expressed as an expansion of orthogonal modes in the form:

$$\begin{Bmatrix}\psi(x,t)\\ w(x,t)\\ \vartheta(x,t)\\ \tau(x,t)\end{Bmatrix} = \sum_k q_k(t)\begin{Bmatrix}\psi_k(x)\\ w_k(x)\\ \vartheta_k(x)\\ \tau_k(x)\end{Bmatrix} \tag{41}$$

where $q_k(t)$ is the modal coordinate. By substitution into Eq. (35), one obtains a first order modal equation of motion:

$$D_k q_k(t) + H_k\frac{d}{dt}q_k(t) = p_k(t) \tag{42}$$

where

$$p_k(t) = \int_{x=0}^{L}p(x,t)w_k(x)dx = \int_{x=0}^{L}P\delta(x-vt)w_k(x)dx = Pw_k(vt) \tag{43}$$

Eq. (42) can be normalized into:

$$\frac{d}{dt}q_k(t) - i\omega_k q_k(t) = \frac{-iP}{2\omega_k M_k^G}w_k(vt) \tag{44}$$

According to [31], this equation is equivalent to:

$$\frac{d^2}{dt^2}q_k(t)+\frac{c}{\mu}\frac{d}{dt}q_k(t)+\omega_k^2 q_k(t)=\frac{P}{\omega_k M_k}w_k(vt) \tag{45}$$

where M_k correspond to the standard modal mass. The solution can be written in fully analytical form (we recall the homogeneous initial conditions):

$$q_j(t)=\frac{P}{M_j^{TH}(\omega_j^{TH})^2}\left(e^{-\xi\omega_j^{TH}t}(q_{AHj}\sin(\omega_{dj}t)+q_{BHj}\cos(\omega_{dj}t))+q_{Aj}\sin\left(\frac{j\pi}{L}vt\right)+q_{Bj}\cos\left(\frac{j\pi}{L}vt\right)\right) \tag{46}$$

where TH designates the theory adopted, either E–B or T–R and

$$\omega_{dj}=\omega_j^{TH}\sqrt{1-\xi^2},\quad \xi=\frac{c}{2\mu\omega_j^{TH}} \tag{47}$$

$$q_{AHj}=\frac{\Omega_j}{\sqrt{1-\xi^2}}\frac{\Omega_j^2+2\xi^2-1}{(2\xi\Omega_j)^2+(1-\Omega_j^2)^2},\quad q_{BHj}=\frac{2\xi\Omega_j}{(2\xi\Omega_j)^2+(1-\Omega_j^2)^2} \tag{48}$$

$$q_{Aj}=\frac{1-\Omega_j^2}{(2\xi\Omega_j)^2+(1-\Omega_j^2)^2},\quad q_{Bj}=\frac{-2\xi\Omega_j}{(2\xi\Omega_j)^2+(1-\Omega_j^2)^2} \tag{49}$$

$$\Omega_j=\frac{j\pi v}{L\omega_j^{TH}} \tag{50}$$

Therefore, it can be seen that the only differences between E–B and T–R beams lie in the modal mass and in the natural frequency, given by (assuming, for simplicity $N=0$):

$$M_j^{E-B}=\frac{1}{2}\mu L \tag{51}$$

$$M_j^{T-R}=\frac{1}{2}\mu L\left(1+r^2\left(\frac{j\pi}{L}-\frac{\mu(\omega_j^{T-R})^2-k}{G\bar{A}}\frac{L}{j\pi}\right)^2\right) \tag{52}$$

When no damping is assumed, Eq. (46) simplifies to:

$$q_j(t)=\frac{P}{M_j^{TH}(\omega_j^{TH})^2(1-\Omega_j^2)}\left[\sin(\Omega_j\omega_j^{TH}t)-\Omega_j\sin(\omega_j^{TH}t)\right] \tag{53}$$

4.3. Critical velocity of a load passing on a finite beam

In this section, the concept of the critical velocity of a load passing on a finite beam will be explained. It will be seen that the critical velocity obtained on a finite beam is an upper approximation of the critical velocity of the corresponding infinite beam. Free vibrations of the beam when the load is already off the structure will also be analysed in this section, because they can exceed the original vibrations.

Let us first consider the case without damping. The maximum value of the jth generalized displacement is given by the resonant formula obtained from Eq. (53) by tending Ω_j to 1:

$$q_{j_r}(t)=\frac{P}{2M_{j_r}^{TH}(\omega_{j_r}^{TH})^2}\left[\sin\left(\omega_{j_r}^{TH}t\right)-\omega_{j_r}^{TH}t\cos\left(\omega_{j_r}^{TH}t\right)\right] \tag{54}$$

This identifies the jth resonant velocity as:

$$v_{j_r}=\frac{L}{j_r\pi}\omega_{j_r}^{TH} \tag{55}$$

which for the E–B beam can be simply written as:

$$v_{j_r}^{E-B}=\frac{L}{j_r\pi}\sqrt{\left(\frac{j_r\pi}{L}\right)^4\frac{EI}{\mu}+\frac{k}{\mu}} \tag{56}$$

Such a resonant velocity can be attributed to each vibration mode. The critical velocity is the lowest resonant velocity, as indicated in [13]. If $v_{j_r}^{E-B}$ in Eq. (56) is considered as a function of j_r, then the minimum value is achieved for a non-integer j_{cr}:

$$j_{cr,1}=\frac{L}{\pi}\sqrt[4]{\frac{k}{EI}},\quad j_{cr,2}=-\frac{L}{\pi}\sqrt[4]{\frac{k}{EI}},\quad j_{cr,3}=i\frac{L}{\pi}\sqrt[4]{\frac{k}{EI}},\quad j_{cr,4}=-i\frac{L}{\pi}\sqrt[4]{\frac{k}{EI}} \tag{57}$$

Substituting $j_{cr,1}$ back in Eq. (56), the critical velocity of the infinite E–B beam is obtained (Eq. (1)), as expected. Thus, the closest integer to $j_{cr,1}$ indicates the critical velocity of the finite E–B beam, which is always higher (at most equal) than the critical velocity of the infinite beam. The same reasoning can confirm Eq. (2).

The resonant generalized coordinate given by Eq. (54) has an envelope linearly increasing with time. Nevertheless, the infinite value is never attained, because Eq. (54) loses its validity when the load leaves the structure. It holds instead:

$$\hat{q}_j(t)=\frac{P\Omega_j}{M_j^{TH}(\omega_j^{TH})^2(1-\Omega_j^2)}\left[\cos(j\pi)\sin\left(\omega_j^{TH}t-\frac{j\pi}{\Omega_j}\right)-\sin(\omega_j^{TH}t)\right] \tag{58}$$

$$\hat{q}_{j_r}(t)=\frac{P}{2M_{j_r}^{TH}(\omega_{j_r}^{TH})^2}[-j_r\pi\cos(\omega_{j_r}^{TH}t)] \tag{59}$$

where the upper "^" indicates that the load is already off the structure.In the case study considered, the 28th mode is the critical one, giving the critical velocity $v_{cr,fin}^{E-B}=205.594$ m/s, which is only 0.01% higher than the critical velocity of the corresponding infinite E–B beam ($v_{cr}^{E-B}=205.573$ m/s). For the T–R beam these values are $v_{cr,fin}^{T-R}=205.272$ m/s and $v_{cr}^{T-R}205.237$ m/s. The 28th mode has thus the highest contribution to the final response when the load passes with the velocity close to the critical one. In Fig. 5, the 28th generalized resonant modal coordinate is shown. It is seen the change in shape at $t=0.97$ s when the load leaves the structure.

The amplitudes of the generalized coordinates are:

$$\tilde{q}_j(t)=\frac{P\Omega_j}{M_j^{TH}(\omega_j^{TH})^2|1-\Omega_j^2|}\sqrt{\cos^2(j\pi)+1-2\cos(j\pi)\cos\left(\frac{j\pi}{\Omega_j}\right)},$$
$$\tilde{q}_{j_r}(t)=\frac{Pj_r\pi}{2M_{j_r}^{TH}(\omega_{j_r}^{TH})^2} \tag{60}$$

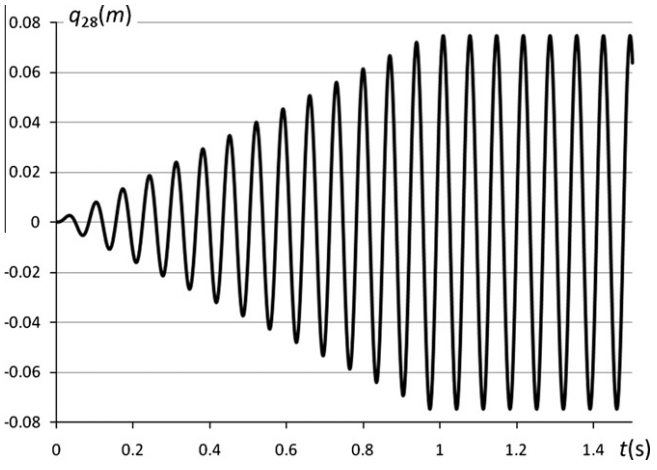

Fig. 5. The generalized 28th resonant modal coordinate.

The maximum amplitude is attained for the integer closest to $j_{mr,1}$, which for the E–B beam is given by:

$$j_{mr,1} = \frac{L}{\pi}\sqrt[4]{\frac{k}{3EI}}, \quad j_{mr,2} = -\frac{L}{\pi}\sqrt[4]{\frac{k}{3EI}},$$
$$j_{mr,3} = i\frac{L}{\pi}\sqrt[4]{\frac{k}{3EI}}, \quad j_{mr,4} = -i\frac{L}{\pi}\sqrt[4]{\frac{k}{3EI}} \tag{61}$$

and for the case study specified is 21. It looks like the maximum displacement of the beam is achieved when the load is off the structure. A more detailed analysis shows that this is verified for displacements directed upward. Regarding the displacement directed downward, higher values are only verified for supercritical velocities. This is caused by the reflected waves having maximum displacements directed upward and downward basically the same. More details are given in Section 6.

When damping is considered, the viscous damping coefficient c from Eq. (45) should consist of the damping contribution that is attributed to the foundation $\tilde{c}$, and to the material damping of the beam itself $\hat{c}.\hat{c}$ is usually expressed by introduction of the modal damping ratio ζ as a ratio of the modal critical damping $2\mu\omega_k$. Thus:

$$c = \tilde{c} + \hat{c} = \tilde{c} + 2\zeta\mu\omega_k \tag{62}$$

It is important to see to what extent such separation influences the final results. In other words, it would be useful to see if there is some connection between the global viscous damping coefficient c and a global modal damping ratio ξ. A first guess would be to define c analogously to the approximate formula for infinite beam as $c = 2\xi\sqrt{k\mu}$, but it can be verified numerically that this is not a good approximation. We suggest instead a new, not yet published, relation as:

$$c = 2\xi\mu\omega_{j_{cr}} = 2\xi\mu\sqrt{\left(\frac{j_{cr}\pi}{L}\right)^4\frac{EI}{\mu} + \frac{k}{\mu}} \cong 2\xi\sqrt{2k\mu} \tag{63}$$

It means that the same level of damping is obtained if either the global modal damping ratio ξ is introduced in a usual way or the viscous damping coefficient c is defined according to Eq. (63). The validity of Eq. (63) is limited to light damping, more or less up to $\xi = 8\%$. This is quite an important result, because then one does not have to pay much attention to separation in Eq. (62). The validity of Eq. (63) was checked numerically. For ξ close to 8%, the maximum displacement directed downward is still quite similar in both cases, but the one directed upward with c-value defined shows sharper asymmetry, and the reflected waves are attenuated more efficiently.

The critical velocity of the damped beam can be defined analogously as in the undamped case. It is useful to remark that it is not usual to define critical velocity for a damped infinite beam. Resonant modal coordinate can be defined as the one that attains its maximum, which means that the term

$$(2\xi\Omega_j)^2 + (1 - \Omega_j^2)^2 \tag{64}$$

must attain its minimum. A simple calculation gives:

$$\Omega_{j_r} = \sqrt{1 - 2\xi^2} \tag{65}$$

Thus, for the E–B beam

$$v_{j_r}^{E-B} = \frac{L\sqrt{1-2\xi^2}}{j_r\pi}\sqrt{\left(\frac{j_r\pi}{L}\right)^4\frac{EI}{\mu} + \frac{k}{\mu}} \tag{66}$$

giving 205.512 m/s for the case study considered and $\xi = 2\%$.

Results between T–R and E–B beams were compared. It is known that, in static analyses, E–B beam theory is valid with sufficient accuracy for $L/h > 10$, where h corresponds to the beam thickness. The T–R theory for dynamic analyses besides shear distortion also introduces the effect of rotary inertia. The higher the vibration mode, the more "waved" is the deflection and therefore these contributions are becoming significant, as seen by comparing Eqs. (31) and (32), and Eqs. (51) and (52). For the case study considered, these differences are plotted in Figs. 6 and 7, up to the 300th mode, as considered for numerical evaluation.

The decrease in the natural frequency for the 300th mode with respect to the E–B formulation is 21.4%, while in the 100th mode only 3.3%. The increase in the modal mass, however, is only 0.87% in the 100th mode and 3.8% in the 300th mode, which for instance for a velocity of 50 m/s indicates only a 0.33% increase in the maximum displacement.

In beams without elastic foundation, the infinite sum in Eq. (14) quickly converges (in E–B beams the modal coordinate is proportional to $1/j^4$), and the first mode has the most significant influence. When the elastic foundation is considered this is not true: the convergence is slower and the most important mode contribution depends on the load velocity. Nevertheless, close to the critical velocity, the major contribution is attributed to the 28th mode, at which, for the case study considered, the differences in frequencies and modal mass are still not important.

By convergence analysis it can be concluded that, for a beam composed of single sub-domain, this number of modes is unnecessarily high (100 modes would be sufficient, the improvement to 300 modes brings only at most 1.5%) but for beam composed of two sub-domains such a high number is necessary.

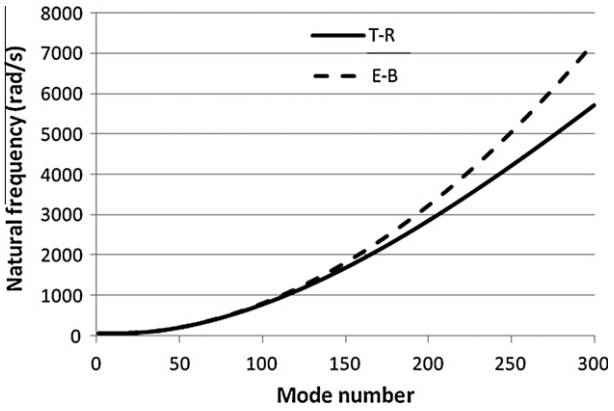

Fig. 6. Natural frequencies for the E–B beam (dashed line) and the T–R beam (solid line).

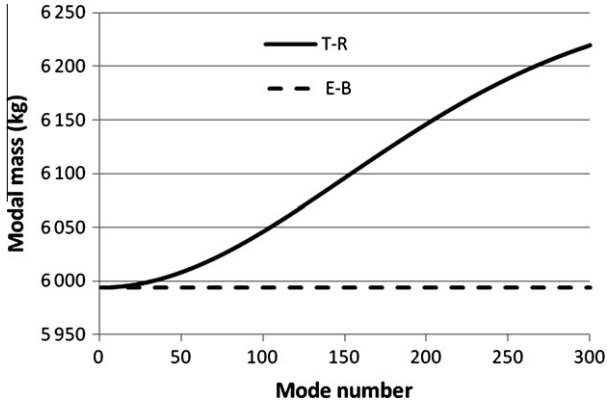

Fig. 7. Modal mass for the E–B beam (dashed line) and the T–R beam (solid line).

5. Beam composed of two sub-domains

5.1. Infinite beam

In order to calculate results corresponding to a infinite beam composed of two sub-domains, the method described in [17] will be used. The region of interest is specified as a 200 m long beam window, separated in two equal lengths of 100 m with foundation stiffness of $k_1 = 0.25$ MN/m^2 and $k_2 = 0.5$ MN/m^2. Only E–B theory is considered. Detailed analysis of formulae presented in [17] confirms that conclusions about resonant and critical velocities presented in Section 4.3 can be extended to beams with a foundation composed of several sub-domains. A resonant velocity $v_{m,r}$ can be attributed to each sub-domain according to:

$$v_{r,m} = \frac{L_m}{\lambda_{r,m}}\sqrt{\left(\frac{\lambda_{m,r}}{L_m}\right)^4\frac{EI}{\mu}+\frac{k_m}{\mu}} \tag{67}$$

where m represents the sub-domain number and $\lambda_{r,m}/L_m$, L_m and k_m are its wave number, length and stiffness of the elastic foundation. The critical velocity is attained for the closest wave number to

$$\frac{\lambda_{cr,m}}{L_m} = \sqrt[4]{\frac{k_m}{EI}} \tag{68}$$

in each sub-domain. This critical velocity is an upper approximation of the critical velocity of the corresponding infinite beam. For the case study considered, the critical velocities of the corresponding infinite beam are $v_{cr,1}^{E-B} = 205.573$ m/s and $v_{cr,2}^{E-B} = 244.47$ m/s, respectively. We recall that in the method described in [17], the actual total beam length must be much larger. In this paper, the total length used was 2000 m and 3000 m for sub- and supercritical velocities, respectively, but this does not affect the conclusions about critical velocities.

5.2. Finite beam

As indicated in Section 3, the total beam length of 200 m is separated in two sub-domains of equal length of 100 m and foundation stiffnesses of $k_1 = 0.25$ MN/m^2 and $k_2 = 0.5$ MN/m^2, respectively. The conclusions about critical velocities are the same as in Section 5.1.

6. Numerical results

6.1. Beam composed of single sub-domain

Analysis of the critical velocity is performed by a parametric analysis with respect to the velocity. The velocity range considered is from 50 m/s to 300 m/s. Velocity step is only 0.1 m/s. Such a small velocity step is necessary in order to represent accurately the waves reflection from the supports in the case of the finite beam. In this case, extreme displacement values are determined from analytical formulas presented in Section 4. Extreme values are extracted from complete results, that are evaluated at every 0.1 m position and every time step that corresponds to an advance of the force by 0.1 m. Since all formulas are analytical, it takes less than 1 s to analyse each velocity case in the Matlab software. Infinite beam results are calculated according to [24]. Extreme displacement values are extracted analytically, and each velocity case is practically instantaneous in the Maple software.

Numerical results are presented in form of graphs. Results were calculated for both E–B as well as T–R beams. There are no visible differences between these results when the load is travelling on the beam, therefore only the ones calculated on E–B beams are shown. For supercritical velocities, slight differences between results were detected in cases when the load is off the structure. These are caused by small differences in imaginary parts of wave numbers that imply slightly different wave length and consequently slightly different instances at which the wave is reflected.

Results summary is presented in Fig. 8 for an undamped case and in Fig. 9 for the case when global damping of $\xi = 2\%$ is considered. Results obtained for the damping coefficient c according to Eq. (63) are not shown because they overlay the previous ones. $\xi = 2\%$ was chosen because 1–3% damping is considered quite realistic value for geomaterials [29]. However, it is necessary to point out that damping coming from the railpads would be much higher [21].

In Fig. 8, solid black lines indicate the extreme values while the load is still on the structure. Let $t_{on} = L/v$ be the time necessary to overpass the beam at velocity v. Curves designated as "off_2", "off_4" and "off_8" identify the extreme values within the time interval $[t_{on}, 2t_{on}]$, $[2t_{on}, 4t_{on}]$ and $[4t_{on}, 8t_{on}]$, respectively. Gray dashed lines report the extreme values of an infinite beam. It can be concluded from Fig. 6, that: (i) for higher velocities, extreme values are highly influenced by wave reflection from supports; (ii) when the load is on the structure, there is only one noticeable peak for downward displacement at $v = 206.2$ m/s (which is slightly different from the analytically determined critical value for finite E–B beam, $v_{cr,fin}^{E-B} = 205.594$ m/s) and for upward displacement at $v = 208.0$ m/s; extreme values in both cases are achieved in locations close to the load position when the force is located close to the right-hand support; (iii) reflected waves imply that higher extreme values are achieved when the load is already off the structure. This is valid for downward displacement at supercritical

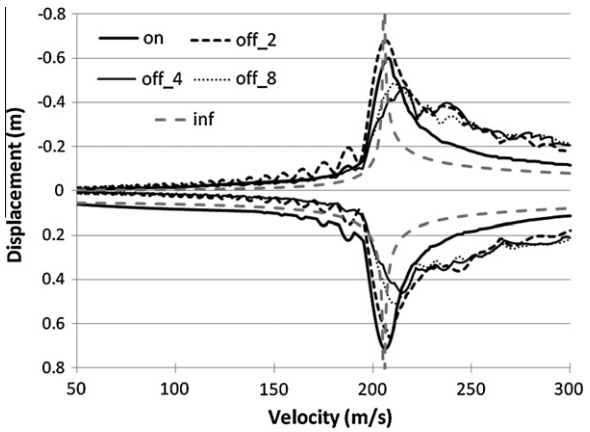

Fig. 8. Analysis of the critical velocity, finite beam, single foundation sub-domain, undamped case.

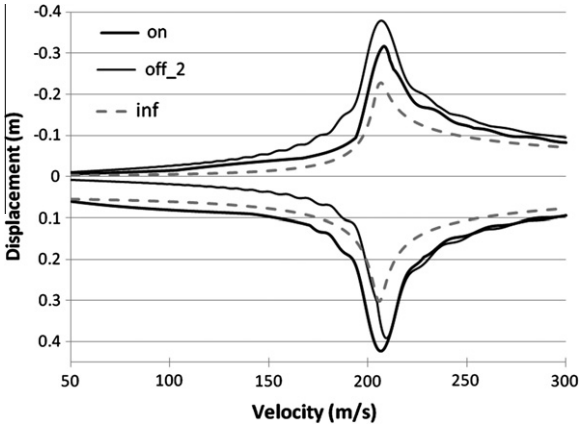

Fig. 9. Analysis of the critical velocity, finite beam, single foundation sub-domain, damped case.

velocities and upward displacement at the full range of velocities. The reason is that reflected waves have downward and upward displacement of the same order of magnitude; and (iv) the maximum displacement gradient is lower than for an infinite beam, it is seen that extreme displacements are very high for velocities around the critical one, while in the case of an infinite beam, there is a very steep increase only very close to the critical velocity.

Analysis of the critical velocities is presented in Fig. 9 for the case of global damping of $\xi = 2\%$. For the infinite beam, the c-value was calculated according to Eq. (63).

It is not usual to define different critical velocities for a damped infinite beam. From the analytical results, the maximum upward and downward displacements are attained for velocities of 205.7 m/s and 206.6 m/s, respectively. For the finite beam, the maximum displacements oriented downward and upward are attained for velocities 206.5 m/s and 208.2 m/s, respectively, when the force is still on the structure. These velocities are higher than the ones reported in the undamped case, although the critical velocity stated analytically should be lower. From Fig. 9, it can be concluded that quite a low level of damping smoothes the curves of results and decreases all values significantly. But again, reflected waves imply that higher extreme values are achieved when the load is already off the structure. This is valid for downward displacement at supercritical velocities and upward displacement at the full range of velocities.

Next two Figs. 10 and 11 exemplify the creation of the reflected wave when $v = 205$ m/s.

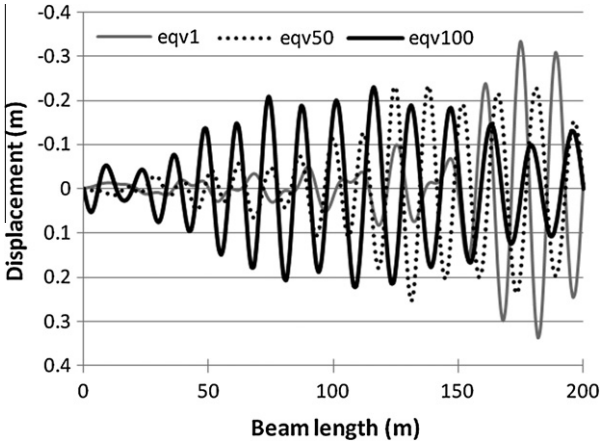

Fig. 10. Creation of the reflected wave, finite beam, single foundation sub-domain, $v = 205$ m/s, undamped case.

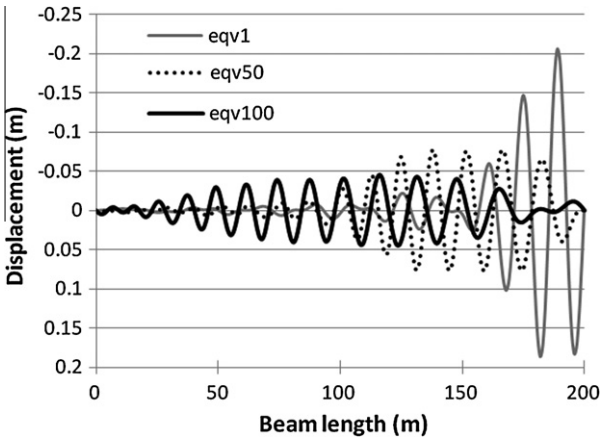

Fig. 11. Creation of the reflected wave, finite beam, single foundation sub-domain, $v = 205$ m/s, damped case.

In the legend of both figures, the number after "eqv" identifies a fictitious length beyond the right-hand support that the force would have travelled off the structure, which according to the load velocity means that the wave is recorded at 0.0049 s, 0.2439 s and 0.4878 s, respectively, after the load has left the beam. It is seen that the highest reflected wave amplitudes occur just after the force leaves the structure. In the damped case, these values are significantly reduced until the new wave reaches the left-hand support. It is seen that the reflected wave has generally the same amplitude oriented downward as upward. This aggravates its negative effect, because the structure is usually designed to resist the displacement field (and the related stress and strain fields) in accordance with the direction of the applied load.

6.2. Beams composed of two sub-domains

In this case, the analysis of critical velocity is also performed by a parametric analysis with respect to the velocity. The velocity range considered is from 50 m/s to 300 m/s. Velocity step is only 0.1 m/s. Displacement values are determined by evaluation analytical formulas reviewed in [17]. Natural frequencies are determined numerically. Extreme displacement values are extracted from complete results that are evaluated at every 1 m. The reason for this rougher scale is the computational time. Due to the high number of modes necessary, significant part of calculation must be executed in Maple software with an increased number of digits precision. This significantly slows down the evaluation. It takes around 15 min to analyse one velocity case in infinite beam and around 3 min in finite beam. It must be stressed that calculations can be done simultaneously. In both cases both software Maple and Matlab are combined together.

Results are presented for infinite and finite beams composed of two sub-domains. For the sake of comparison, results of two infinite beams composed of single sub-domain of elastic foundations $k_1 = 0.25$ MN/m^2 and $k_2 = 0.5$ MN/m^2 are also included in order to better compare the predicted critical velocities, that are $v_{cr,1}^{E-B} = 205.573$ m/s and $v_{cr,2}^{E-B} = 244.47$ m/s according to Eq. (1). Summary of the results is presented in Figs. 12 and 13 for the undamped case and in Figs. 14 and 15 for the damped one on the infinite beam, and in Figs. 16 and 17 for the undamped case and in Figs. 18 and 19 for the damped one on the finite beam. In each case, results are separated in two figures and four double curves according to the load position and according to the position of the extreme displacement, because it is important to see the effect of the transition radiation that occurs after crossing the sub-domains common point.

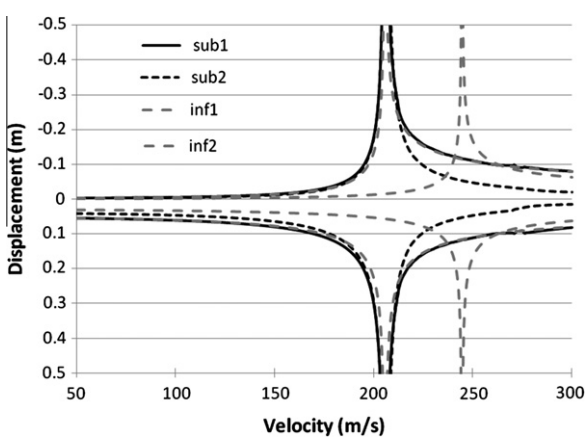

Fig. 12. Analysis of the critical velocity, infinite beam, two sub-domains, undamped case, load position in sub-domain 1.

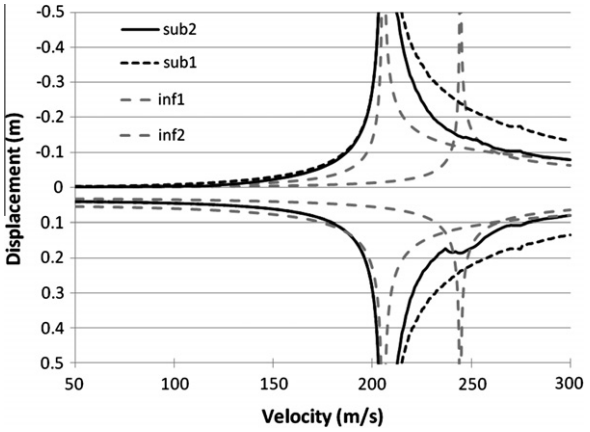

Fig. 13. Analysis of the critical velocity, infinite beam, two sub-domains, undamped case, load position in sub-domain 2.

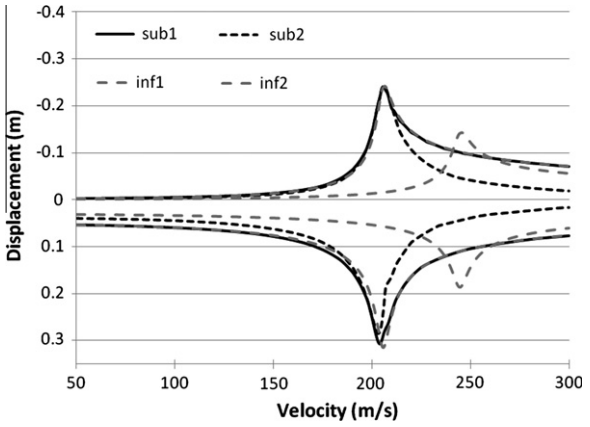

Fig. 14. Analysis of the critical velocity, infinite beam, two sub-domains, damped case, load position in sub-domain 1.

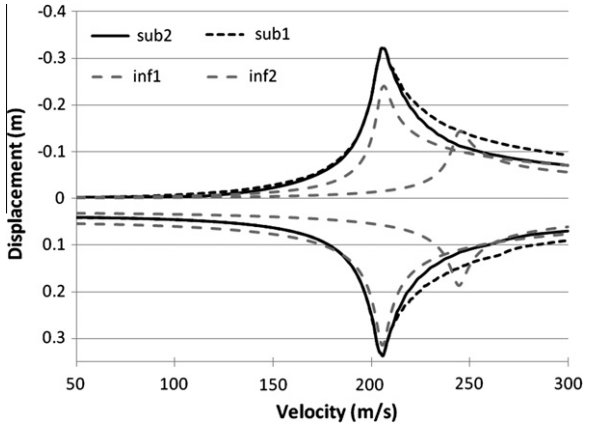

Fig. 15. Analysis of the critical velocity, infinite beam, two sub-domains, damped case, load position in sub-domain 2.

In the following, results related to infinite beams are presented. There are no reflected waves perturbing the results, as expected. Therefore, the influence of the transition radiation can be analysed better than in the finite beam cases.

As already mentioned, extreme values are recorded separately in each sub-domain, specified in the figures legend "sub1" and "sub2". However, when the extreme value is achieved in the common position, it will be attributed to both sub-domains. Extreme values in the same sub-domain as the load position are represented by solid black lines, the other extreme values are designated by short-dashed lines. Extreme values of two distinct infinite beams are given by gray long-dashed lines.

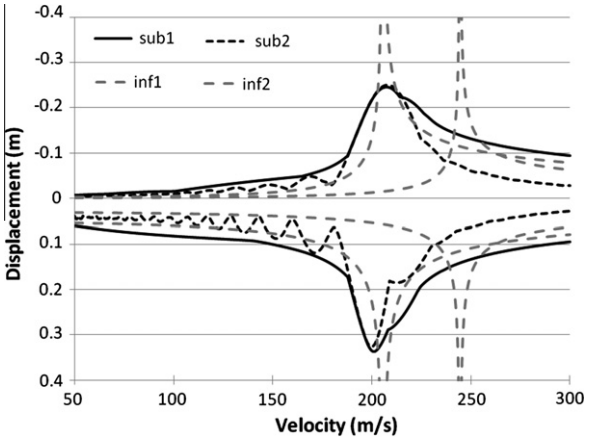

Fig. 16. Analysis of the critical velocity, finite beam, two sub-domains, undamped case, load position in sub-domain 1.

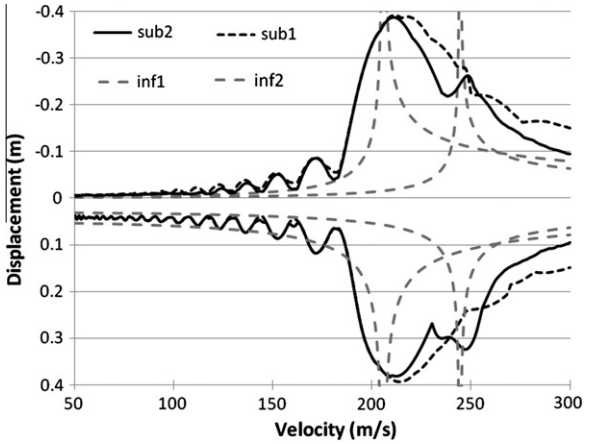

Fig. 17. Analysis of the critical velocity, finite beam, two sub-domains, undamped case, load position in sub-domain 2.

When the force travels over sub-domain 1, extreme values in sub-domain 1 practically follow the results of the first infinite single beam. Extreme values in sub-domain 2 have a similar tendency, but are lower.

When the force traverses the second sub-domain, the tendency of the first infinite single beam is again followed, only in an augmented version due to the transition radiation. The second critical velocity is hardly noticeable. Contrary to what happens in the finite beam, infinite displacements are attained.

Global damping of $\xi = 2\%$ is used for results presented in Fig. 15. Results are similar to the undamped case, but the displacement values are considerably lower, and infinite displacements are not attained.

Figs. 16–19 pertain to the results obtained in finite beams. The same legend scheme as before is used. When the force is still over the softer sub-domain, the harder region already exhibits the critical velocity of the softer sub-domain. When the force is already passing over the harder region, both critical velocities are clearly marked there. Thus, the harder sub-domain that has a higher critical velocity "gains" another displacement peak that corresponds to the critical velocity of the softer sub-domain.

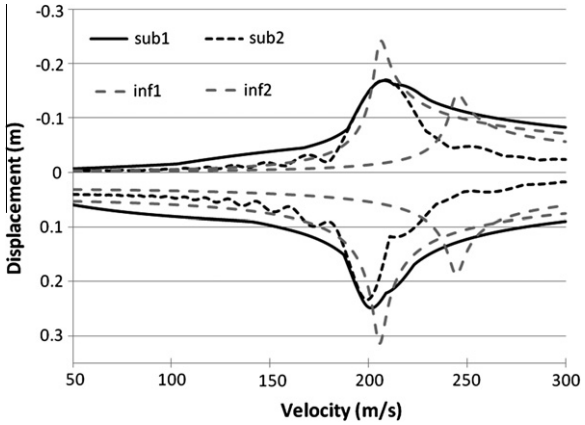

Fig. 18. Analysis of the critical velocity, finite beam, two sub-domains, damped case, load position in sub-domain 1.

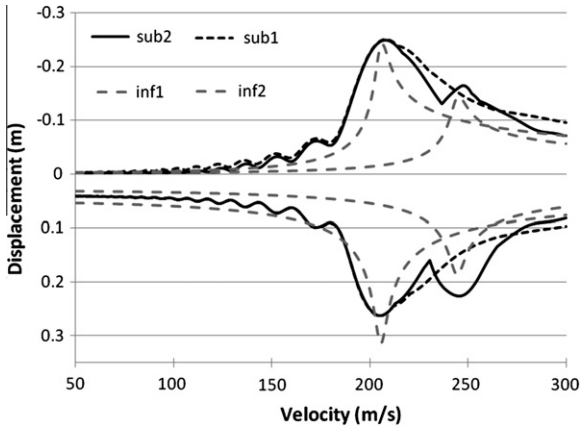

Fig. 19. Analysis of the critical velocity, finite beam, two sub-domains, damped case, load position in sub-domain 2.

It can be concluded by comparison of Figs. 16 and 17, that extreme values in sub-domain 1 are higher when the load is travelling over sub-domain 2 than when it is travelling over sub-domain 1.

Analogous conclusions can be drawn in the damped case. The same legend scheme as before is used, the only difference being that displacements are significantly lower.

The main difference between the finite beam and the infinite beam is seen when comparing this last Fig. 19 with Fig. 15. For the infinite beam, in the damped case, it looks like the harder region looses its critical velocity. In both Figs. 14 and 15, only the lower critical velocity is marked in both sub-domains. This means that the influence of the transition radiation is so strong that it takes some time until the wave is stabilized into its quasi-steady form over the stronger region. This stabilization occurs already outside the region of interest.

From all Figs. 13, 14, 17 and 19, i.e. from the ones that are related to the load passage over the harder sub-domain, it is seen that when extreme displacements are reached they have practically the same value in the downward as well as upward direction.

7. Conclusions

In this paper, the analysis of the critical velocity of a load moving uniformly along a beam on a visco-elastic foundation was presented. The critical velocity is defined as the load velocity inducing the beam highest deflections directed downward and/or upward. The study was carried out through a parametric analysis which aimed to obtain the highest displacements attained in the beam as a function of the load velocity. Both finite and infinite beams were considered, as were foundations composed of one or two sub-domains, and the presence or absence of damping was also accounted for. The analysis was not focused exclusively in the time span the load takes to traverse the beam, but also registered the displacements due to the free vibrations after the load is off the beam. The case study addressed is of interest to high-speed railway lines, particularly for abrupt changes in the foundation stiffness.

Among the developments presented in this paper, new formulations are given for: (i) the first order state-space form of T–R beam; and (ii) for the relation between the viscous damping constant and the modal damping ratio assuring the same level of damping in lightly damped finite beam structures.

Small differences between the analytically predicted critical velocities and the velocities that lead to numerically extreme values were observed. However, since these differences range around 1% or less, the analytical expressions can still be regarded as suitable predictions of the critical velocity.

It was shown that results obtained on a finite beam on soft visco-elastic foundation cannot be interchanged with results obtained on a corresponding infinite beam. In infinite beams, extreme displacements as a function of the velocity only exhibit a sharp increase for values very close to the critical velocity. In finite beams, extreme displacement increase more gradually and the effect of reflections from supports is non-negligible.

In finite beams composed of one sub-domain, extreme values are achieved in locations close to the load position when the force is located close to the right-hand support. In addition, reflected waves imply that higher extreme values are achieved when the load is already off the structure. This is valid for downward displacement at supercritical velocities and upward displacement at the full range of velocities. The reason is that reflected waves have downward and upward displacement of the same order of magnitude. Even a low level of damping is enough to smooth the resulting extreme displacements curves and significantly decreases all values.

In finite beams composed of two sub-domains, when the force passes over the softer sub-domain, the harder region already exhibits augmented displacements for the critical velocity of the softer sub-domain. When the force is passing over the harder region, both critical velocities are clearly marked due to the transition radiation. Thus, the harder sub-domain, that has a higher critical velocity, "gains" another displacement peak that corresponds to the critical velocity of the softer sub-domain. It was also observed that extreme values in the first sub-domain are higher when the force was travelling over the second sub-domain than when it was travelling over the first sub-domain.

In the Figures that represent the load passage over the harder sub-domain (Figs. 13, 15, 17 and 19), it is seen that, when extreme displacements are reached, they have practically the same value in the downward as well as the upward direction, which confirms that these extreme displacements are the result of transition radiation.

The results obtained can have direct application on the analysis of railway track vibrations induced by high-speed trains when crossing regions with significantly different foundation stiffness. The critical velocities determined for the case study considered are still unattainable by nowadays trains, but the results presented in this paper have practical importance because they show values of extreme displacements as a function of velocity. This type of analysis can be used to identify augmented displacements directed upward, that aggravate track deterioration. These occurrences should be avoided in railway applications, because the structure is usually designed to resist the displacement field (and the related

stress and strain field) in accordance with the direction of the applied load, i.e. downward.

Acknowledgements

The authors greatly appreciate the support from Fundação para a Ciência e a Tecnologia, of the Portuguese Ministry of Science and Technology under the Grant PTDC/EME-PME/01419/2008: "SMARTRACK – SysteM dynamics Assessment of Railway TRACKs: a vehicle-infrastructure integrated approach".

References

[1] Dimitrovová Z, Varandas JN. Critical velocity of a load moving on a beam with a sudden change of foundation stiffness: applications to high-speed trains. Comput Struct 2009;87:1224–32.
[2] Krylov AN. Über die erzwungenen Schwingungen von gleichformigen elastichen Stäben. Mathematische Annalen 1905;61:211–34. in German.
[3] Timoshenko SP. Forced vibration of prismatic bars. Izvestiya Kievskogo politekhnicheskogo instituta [in Russian], 1908; Erzwungene Schwingungen prismatischer Stabe. Zeitschrift für Mathematik und Physik 1911;59(2): 163–203. in German.
[4] Inglis CE. A mathematical treatise on vibration in railway bridges. Cambridge: The Cambridge University Press; 1934.
[5] Lowan AN. On transverse oscillations of beams under the action of moving variable loads. Phil Mag 1935;19(127):708–15. Series 7.
[6] Koloušek V. Dynamics of civil engineering structures—Part I: General problems, 2nd ed.—Part II: Continuous beams and frame systems, 2nd ed.—Part III: Selected topics, SNTL, Prague, 1967, 1956, 1961 [in Czech]. Dynamics in Engineering Structures, Academia, Prague, Butterworth, London; 1973.
[7] Frýba L. Vibration of solids and structures under moving loads, Research Institute of Transport, Prague (1972). 3rd ed. London: Thomas Telford; 1999.
[8] Andrews LC, Shivamoggi BK. Integral transforms for engineers and applied mathematicians. New York: Macmillan Publishing Company; 1988.
[9] Timoshenko SP. Statical and dynamical stresses in rails. Proceedings of the 2nd international congress for applied mechanics. Zürich (Switzerland); 12–17 September 1926. p. 407–18.
[10] Kenney Jr JT. Steady-state vibrations of beam on elastic foundation for moving load. ASME J Appl Mech 1954;21:359–64.
[11] Frýba L. Infinite beam on an elastic foundation subjected to a moving load. Aplikace Matematiky 1957;2(2):105–32. in Czech.
[12] Choros J, Adams GG. A steadily moving load on an elastic beam resting on a tensionless Winkler foundation. ASME J Appl Mech 1979;46:175–80.
[13] Chen Y-H, Huang Y-H. Dynamic characteristics of infinite and finite railways to moving loads. ASCE J Eng Mech 2003;129(9):987–95.
[14] Vesnitskii AI, Metrikine AV. Transition radiation in mechanics. Physics – Uspekhi 1996;39:983–1007.
[15] van Dalen KN, Metrikine AV. Transition radiation of elastic waves at the interface of two elastic half-planes. J Sound Vib 2008;310:702–17.
[16] Van Dalen KN. Ground vibration induced by a high-speed train running over inhomogeneous subsoil. Transition radiation in two-dimensional inhomogeneous elastic systems. Master thesis, Department of Structural Engineering, TUDelft; 2006.
[17] Dimitrovová Z. A general procedure for the dynamic analysis of finite and infinite beams on piece-wise homogeneous foundation under moving loads. J Sound Vib 2010;329:2635–53.
[18] Rodrigues AFS. Transverse vibrations in finite beams subjected to moving loads – transition radiation associated to abrupt change in foundation vertical stiffness. Master thesis, Department of Civil Engineering, Universidade Nova; 2010 [in Portuguese].
[19] Chen J-S, Chen Y-K. Steady state and stability of a beam on a damped tensionless foundation under a moving load. Int J Non-Linear Mech 2011;46:180–5.
[20] Wu L, Wen ZF, Xiao XB, Li W, Jin XS. Modeling and analysis of vehicle-track dynamic behavior at the connection between floating slab and non-floating slab track. In: Topping BHV, Adam JM, Pallarés FJ, Bru R, Romero ML, editors. Proceedings of the tenth international conference on computational structures technology. Paper 20. Stirlingshire, UK: Civil-Comp Press; 2010. doi:10.4203/ccp. 93.20.
[21] Nielsen JCO, Oscarsson J. Simulation of dynamic train–track interaction with state-dependent track properties. J Sound Vib 2004;275:515–32.
[22] Andersen L. Do lumped-parameter models provide the correct geometrical damping? DCE Technical Memorandum No. 5, Department of Civil Engineering, Aalborg University, Denmark; 2007. ISSN 1901–7278.
[23] Clough RW, Penzien J. Dynamics of structures. 3rd ed. USA: Computers & Structures, Inc.; 2003.
[24] Chen YH, Huang Y-H. Dynamic stiffness of infinite Timoshenko beam on viscoelastic foundation in moving co-ordinate. Int J Numer Methods Eng 2000;48:1–18.
[25] Gartner JR, Olgac N. Improved numerical computation of uniform beam characteristic values and characteristic functions. J Sound Vib 1982;84:481–9.
[26] Goncalves PJP, Brennan MJ, Elliott SJ. Numerical evaluation of high-order modes of vibration in uniform Euler–Bernoulli beams. J Sound Vib 2007;301:10351039.
[27] Release 11 Documentation for MAPLE, Maplesoft a Division of Waterloo Maple, Inc.; 2007.
[28] Release R2007a Documentation for MATLAB, The MathWorks, Inc.; 2007.
[29] A case study definition of a railway track for the numerical simulation, Internal report on POCI/ECM/61114/2004 grant. Minho University, Portugal; 2006 [in Portuguese].
[30] Dimitrovová Z. Dynamic analysis of beam structures under moving loads: a review of the modal expansion method. In: Topping BHV, Tsompanakis Y, editors. Civil and structural engineering computational technology. Stirlingshire, UK: Saxe-Coburg Publications; 2011. p. 99–130. doi:10.4203/csets.28.4, [chapter 4].
[31] Krenk S. Complex modes and frequencies in damped structural vibrations. J Sound Vib 2004;270:981–96.